SIAM J. SCI. COMPUT.
Vol. 46, No. 6, pp. A3703–A3726

SHAPE OPTIMIZATION UNDER A CONSTRAINT ON THE WORST-CASE SCENARIO*

FABIEN CAUBET‡, MARC DAMBRINE†, GIULIO GARGANTINI§, AND JÉRÔME MAYNADIER¶

Abstract. This work falls within the general framework of robust shape optimization under constraints, where a physical parameter of the problem is poorly known. In particular, we study problems where one of the constraints concerns the maximal possible value that a given shape functional can assume when the uncertain parameter varies within an admissible range. Two different approaches are considered: the first one based on the approximation of the set of admissible uncertain parameters by a convex polyhedron, and the second one relying on the notion of subdifferential in the sense of Clarke. The main contributions of this work consist in the theoretical proof of convergence of the first approach under suitable hypotheses of convexity of the set of admissible parameters and of the constraint, and the adaptation of Clarke's subdifferential in the context of robust shape optimization. The two techniques are compared numerically in three examples, with the objective of minimizing the volume of elastic structures under a constraint on the worst-case scenario for the mechanical compliance and the von Mises stress.

Key words. shape optimization under uncertainties, worst-case optimization, shape derivatives, subdifferential, robustness

MSC codes. 49Q10, 65K05, 65N99, 35Q93, 90C70

DOI. 10.1137/24M1648818

1. Introduction.

In this work we focus on the optimization of linear elastic structures subjected to uncertain mechanical loads. Several different approaches can be contemplated in order to take uncertain parameters into account. If some information on the probability distribution of the uncertainties is available, techniques of robust topology optimization (RTO) or reliability-based topology optimization (RBTO) can be considered. See [35, 18, 4, 22, 25, 23] for more information on the different approaches to RTO and RBTO problems. As reported in [14], the optimization of the worst-case scenario is preferable to other approaches involving stochastic quantities when the data are imprecise or if they are uncertain with an unknown probability distribution, or if the strict respect of the constraint in all circumstances is of primary importance. In many industrial applications, safety is a critical issue and the strict respect of the constraint in all circumstances is of primary importance. Any probabilistic criterion to measure the risk of failure cannot be used in this context. Therefore, in this paper we focus on a worst-case criterion.

Problem statement. Let us study the following shape optimization problem, where the objective consists in the minimization of the volume of the structure under mechanical constraints. We consider a structure represented by a Lipschitz continuous

*Submitted to the journal's Numerical Algorithms for Scientific Computing section March 25, 2024; accepted for publication (in revised form) August 27, 2024; published electronically December 3, 2024.

https://doi.org/10.1137/24M1648818

†E2S UPPA, CNRS, LMAP, UMR 5142, Université de Pau et de Pays de l'Adour, Pau, 64000, France (marc.dambrine@univ-pau.fr).

‡LMAP, UPPA, Pau, 64013, France (fabien.caubet@univ-pau.fr).

§E2S UPPA, CNRS, LMAP, UMR 5142, Université de Pau et de Pays de l'Adour, Pau, 64000, France, and Safran Helicopter Engines, Bordes, 64510, France (giulio.gargantini@univ-pau.fr).

¶Safran Helicopter Engines, Bordes, 64510, France (jerome.maynadier@safrangroup.com).

bounded domain $\Omega \subset \mathbb{R}^d$, with $d = 2$ or $d = 3$. We suppose its boundary $\partial\Omega$ to be divided in three disjoint parts with strictly positive measure: Γ_{D}, Γ_{N}, and Γ_0. The structure is clamped in Γ_{D}, and a force $\mathbf{g}$ is applied on Γ_{N}. The displacement solves the following linear elasticity equations:

$$\left\{\begin{array}{rl} -\mathrm{div}\left(\boldsymbol{\sigma}\left(\mathbf{u}_{\Omega,\mathbf{g}}\right)\right) = \mathbf{f} & \text{in } \Omega, \\ \boldsymbol{\sigma}\left(\mathbf{u}_{\Omega,\mathbf{g}}\right)\mathbf{n} = \mathbf{g} & \text{on } \Gamma_{\mathrm{N}}, \\ \boldsymbol{\sigma}\left(\mathbf{u}_{\Omega,\mathbf{g}}\right)\mathbf{n} = \mathbf{0} & \text{on } \Gamma_0, \\ \mathbf{u}_{\Omega,\mathbf{g}} = \mathbf{0} & \text{on } \Gamma_{\mathrm{D}}. \end{array}\right. \tag{1.1}$$

Here $\boldsymbol{\sigma}\left(\mathbf{u}_{\Omega,\mathbf{g}}\right)$ denotes the stress tensor which is taken, according to Hooke's law, as a linear function of the linearized strain tensor $\boldsymbol{\varepsilon}\left(\mathbf{u}_{\Omega,\mathbf{g}}\right)$ defined as the symmetric part of the gradient of the displacement. For a homogeneous isotropic material, the linear relation between the stress and strain tensors is given by

$$\boldsymbol{\sigma}\left(\mathbf{u}_{\Omega,\mathbf{g}}\right) = 2\mu\boldsymbol{\varepsilon}\left(\mathbf{u}_{\Omega,\mathbf{g}}\right) + \lambda(\mathrm{div}\,\mathbf{u}_{\Omega,\mathbf{g}})\mathbb{I},$$

where $\mathbb{I}$ is the identity matrix, and μ and λ are the Lamé parameters.

In this work we assume that the mechanical loads applied are uncertain. Let us suppose that $\mathbf{f}$ belongs to $\mathrm{L}^2\left(\Omega\right)^d$ and that $\mathbf{g}$ is a parameter that belongs to a bounded set $\mathcal{G} \subset \mathrm{L}^2\left(\Gamma_{\mathrm{N}}\right)^d$. Then we consider the following generic constrained optimization problem defined on the set of admissible shapes $\mathcal{S}_{\mathrm{adm}}$ which will be specified below:

$$\left|\begin{array}{l} \text{Find the admissible shape } \Omega \in \mathcal{S}_{\mathrm{adm}} \text{ minimizing the volume } \mathrm{Vol}(\Omega) \\ \text{under the constraint } \sup_{\mathbf{g}\in\mathcal{G}} H(\mathbf{u}_{\Omega,\mathbf{g}}, \Omega) \leq \tau, \\ \text{where the displacement } \mathbf{u}_{\Omega,\mathbf{g}} \in \mathrm{H}^1_{\Gamma_{\mathrm{D}}}\left(\Omega\right)^d \text{ solves (1.1).} \end{array}\right. \tag{1.2}$$

Here and in the following, τ denotes a given threshold not to be exceeded. Finally, we assume that the considered constraint functional $H(\cdot,\cdot)$ is written in integral form as

$$H(\mathbf{u}, \Omega) = \int_\Omega \left(j_0(\mathbf{u}(\mathbf{x})) + j_1(\nabla\mathbf{u}(\mathbf{x}))\right) \mathrm{d}\mathbf{x} \qquad \text{for } \mathbf{u} \in \mathrm{H}^1\left(\Omega\right)^d, \tag{1.3}$$

with j_0 and j_1 continuous functions. If the mapping $\mathbf{g} \mapsto H(\mathbf{u}_{\Omega,\mathbf{g}}, \Omega)$ is continuous and the set $\mathcal{G}$ is compact, $H(\mathbf{u}_{\Omega,\mathbf{g}}, \Omega)$ reaches its supremum for some $\mathbf{g} \in \mathcal{G}$, and the constraint can be replaced by $\max_{\mathbf{g}\in\mathcal{G}} H(\mathbf{u}_{\Omega,\mathbf{g}}, \Omega) \leq \tau$.

State of the art. As remarked in [3], two different points of view can be adopted, according to whether the functional affected by the perturbation acts as the objective of an optimization problem or as a constraint. If the objective of the optimization is the minimization of the maximal possible level of a functional, the problem can be formulated as a *min-max* problem. This interpretation can also be applied to the case of constrained optimization problems where an upper bound on the maximum of a functional is imposed. However, this constraint can also be interpreted as imposing an upper bound on the constraining functional for all possible configurations of the uncertain parameters.

Different techniques to solve shape optimization problems with worst-case functionals have been proposed. In [20, 31, 42, 7] the objective of the optimization problem consists in minimizing the maximal possible value of a given functional. In particular, the studies of Cherkaev and Cherkaev [20], and of de Gournay, Allaire, and Jouve [31] focus on minimizing the *robust compliance* of an elastic structure subject to an uncertain load by taking advantage of the convexity of that specific functional. In [36, 3, 7]

are considered also problems where the uncertain functional acts as a constraint, and numerical examples are provided for density and level-set methods. The authors of [3] consider smooth functionals subject to small perturbations and propose a method to compute the shape derivative of their supremum using linearization techniques. This approach was slightly improved in [26]. For further information about worst-case problems, outside the domain of structure optimization, we refer the reader to [14, 13].

Contribution and organization of the paper. In this paper, two different methods for solving shape optimization problems under worst-case scenario constraints for a given functional are presented and compared. Contrarily to the approach of [3], no assumptions on the size uncertainties are asserted. However, both methods require the convexity of the constraint functional with respect to the displacement.

In industrial applications, the principal technique to approximate the solution of problem (1.2) consists in the identifying a number N of representative loading conditions and considering them as separate constraints of the shape optimization problem. In section 2 we study that method and provide our first contribution in Theorem 2.7: as N goes to infinity, this approach provides a sequence of minimizers that converges to a domain solving the original problem. For this purpose, we assume convexity of both the constraint functional and the set of allowable mechanical loads. In section 3 we study a general approach based on Clarke's subdifferentials dealing with the nondifferentiability of a supremum. In that context, we provide in Proposition 3.2 the expression of the shape subdifferential. Finally, in section 4 the results of the two methods are compared for some numerical applications in three dimensions.

2. A multiscenario approach for the worst case.

In this section, convexity is the essential tool preventing assumptions on the small amplitude of uncertainties. More precisely, we will use the fact that the ambiguous set for the loading is a convex compact set in a finite-dimensional space and that the constraint is a convex function of the displacement.

2.1. The chosen topology on sets and the continuity of the constraints.

Before describing the first approach, we recall classical facts. First, we shall utilize a classical result often referred to as Bauer's maximum principle, concerning the maximization of convex functionals on convex sets. Such a result descends directly from [45, Theorem 32.3] and its corollaries.

PROPOSITION 2.1. *Let $f : \mathcal{X} \to \mathbb{R}$ be a convex and bounded function defined on the Banach space $\mathcal{X}$, and let $\mathcal{S} \subset \mathcal{X}$ be a compact convex set. Then f attains $\sup_{\mathbf{x}\in\mathcal{S}} f(\mathbf{x})$ in at least a point $\bar{\mathbf{x}} \in \mathcal{S}$, belonging to the border $\partial\mathcal{S}$ of the set $\mathcal{S}$. Moreover, if $\mathcal{S}$ is a convex, closed, and bounded polyhedral set, $\bar{\mathbf{x}}$ can be found among the vertices of $\mathcal{S}$.*

In order to define the concept of convergence for the domains, it is necessary to introduce a topology on the set of admissible shapes $\mathcal{S}_{\mathrm{adm}}$ and among the sets of possible mechanical loads. We recall the notion of Hausdorff distance between subsets of metric spaces as in [39, Definition 2.2.7]; see also [9, Proposition 1.2].

DEFINITION 2.2 (Hausdorff distance). *Let $\mathcal{M}$ be a metric space provided with the distance $\mathrm{d}_{\mathcal{M}}$, and let $\mathcal{A}_1$ and $\mathcal{A}_2$ be two compact subsets of $\mathcal{M}$. The Hausdorff distance between the sets $\mathcal{A}_1$ and $\mathcal{A}_2$ is*

$$\mathrm{d_H}(\mathcal{A}_1, \mathcal{A}_2) = \max\left\{ \sup_{\mathbf{x}\in\mathcal{A}_1} \mathrm{d}_{\mathcal{M}}(\mathbf{x}, \mathcal{A}_2),\ \sup_{\mathbf{y}\in\mathcal{A}_2} \mathrm{d}_{\mathcal{M}}(\mathbf{y}, \mathcal{A}_1) \right\}.$$

In order to define a metric and the notion of convergence for open subsets of $\mathcal{M}$, we limit our study to uniformly bounded open sets. Let $\mathcal{B} \subset \mathcal{M}$ be a fixed compact subset of $\mathcal{M}$. We consider the Hausdorff metric on the class of the open subsets of $\mathcal{B}$ as proposed in [39, Definition 2.2.8 and Remark 2.2.10].

The shape functional $\Omega \mapsto \sup_{\mathbf{g}\in\mathcal{G}} H(\mathbf{u}_{\Omega,\mathbf{g}}, \Omega)$ is not continuous if $\mathcal{S}_{\text{adm}}$ is a generic class of open domains in $\mathbb{R}^d$, since it relies on the computation of $\mathbf{u}_\Omega$. Therefore, we can restrict the class of admissible domains to domains satisfying the ε-cone condition (see [39, Definition 2.4.1]). The continuity of $\Omega \in \mathcal{S}_{\text{adm}} \mapsto \sup_{\mathbf{g}\in\mathcal{G}} H(\mathbf{u}_{\Omega,\mathbf{g}}, \Omega) \in \mathbb{R}$ relies on the following result, proven in [19] and reported in [39, Theorem 3.2.13].

THEOREM 2.3. *We consider $\varepsilon > 0$, and $\mathcal{B} \subset \mathbb{R}^d$ to be a compact set. Let $\{\Omega_n\}_{n=1}^{\infty}$ and Ω be open domains in $\mathcal{S}_{\text{adm}} \subset \mathcal{D}_\varepsilon(\mathcal{B})$, and let $\Omega_n \xrightarrow{\text{H}} \Omega$. Then the sequence $\{\mathbf{u}_{\Omega_n}\}_{n=1}^{\infty}$ converges towards $\mathbf{u}_\Omega$, where $\mathbf{u}_\Omega$ is the solution of the linear elasticity problem on Ω and $\mathbf{u}_{\Omega_n}$ is the solution on Ω_n for all $n \geq 0$.*

Theorem 2.3, combined with the structure of the constraint stated in (1.3), ensures that the shape functional $\Omega \mapsto \sup_{\mathbf{g}\in\mathcal{G}} H(\mathbf{u}_{\Omega,\mathbf{g}}, \Omega)$ is continuous on a class of uniformly bounded open sets satisfying the ε-cone condition for some positive ε.

2.2. Main theoretical results. From now on, we consider that all admissible domains satisfy the ε-cone condition, that they are uniformly bounded by a compact set $\mathcal{B}$, and that $\mathcal{S}_{\text{adm}}$ is a closed subset of $\mathcal{D}_\varepsilon(\mathcal{B})$ for some $\varepsilon > 0$. We suppose that the set of admissible loads is bounded, convex, and finite-dimensional, and the mapping $\mathbf{g} \mapsto H(\mathbf{u}_{\Omega,\mathbf{g}}, \Omega)$ is a convex function. The objective of this section is to justify the approach of the engineers and provide some results on the convergence of the solution when the number of loading conditions N increases.

We state all the results of this section for the following generic optimization problem, where the dependence from the state is kept implicit:

$$\left|\begin{array}{l} \text{Find the admissible shape } \Omega \in \mathcal{S}_{\text{adm}} \text{ minimizing the volume } \operatorname{Vol}(\Omega) \\ \text{under the constraint } \sup_{\mathbf{g}\in\mathcal{G}} h(\mathbf{g}, \Omega) \leq \tau\,. \end{array}\right. \tag{2.1}$$

We suppose that $\mathcal{G}$ is a compact convex set contained in a finite-dimensional space $(\mathcal{Y}, \|\cdot\|_{\mathcal{Y}})$, and that $h : \mathcal{G} \times \mathcal{S}_{\text{adm}} \to \mathbb{R}$ is a real-valued function. The mapping $\Omega \mapsto h(\mathbf{g}, \Omega)$ can be seen as an instance of a family of shape functions depending on the parameter $\mathbf{g} \in \mathcal{G}$. Moreover, we assume that the functions satisfy the following conditions:

(i) the mapping $\mathbf{g} \mapsto h(\mathbf{g}, \Omega)$ is convex and bounded for all admissible $\Omega \in \mathcal{S}_{\text{adm}}$;
(ii) for all choices of the parameter $\mathbf{g} \in \mathcal{G}$, the mapping $\Omega \mapsto h(\mathbf{g}, \Omega)$ is shape differentiable.

A first result on the solution of problem (1.2) is provided by the following proposition, which applies to the case where the set of admissible loads is polyhedral.

PROPOSITION 2.4. *Let $\mathcal{G}$ be a compact convex polyhedral subset of the Banach space $\mathcal{Y}$ with N vertices $\mathbf{g}_1, \ldots, \mathbf{g}_N$, and let $h : \mathcal{G} \times \mathcal{S}_{\text{adm}} \to \mathbb{R}$ be a real-valued function satisfying assumptions* (i)–(ii) *stated above. Then the solution of problem* (2.1) *is equivalent to the solution of the following constrained optimization problem:*

$$\left|\begin{array}{l} \textit{Find the admissible shape } \Omega \in \mathcal{S}_{\text{adm}} \textit{ minimizing the volume } \operatorname{Vol}(\Omega) \\ \textit{under the } N \textit{ inequality constraints: } \forall i \in \{1, \ldots, N\},\ h(\mathbf{g}_i, \Omega) \leq \tau\,. \end{array}\right. \tag{2.2}$$

Proposition 2.4 follows directly from the application of Proposition 2.1 to the inequality constraint. Moreover, the formulation of Proposition 2.1 as an optimization

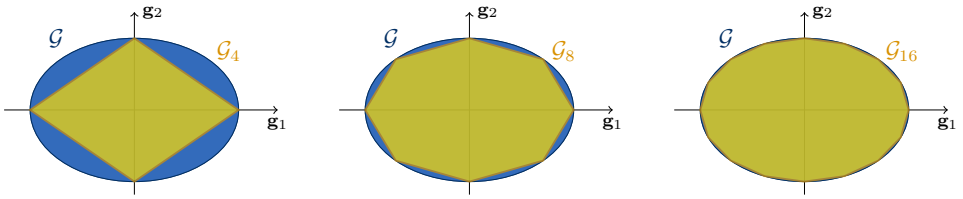

(a) $N = 4$ (b) $N = 8$ (c) $N = 16$

FIG. 1. *Approximation of the set of admissible parameters by convex polyhedra with an increasing number of vertices N.*

problem with multiple constraints makes it conforming with the *nullspace optimization algorithm* introduced in [34, 33], which simplifies the numerical implementation.

Having proven a result on the solution of problem (2.1) for convex polyhedra, we aim to extend it to more general compact convex sets. Let $\mathcal{G}$ be a compact and convex subset of a Banach space $\mathcal{Y}$, and let $\{\mathcal{G}_n\}_{n=1}^{\infty}$ be a sequence of convex compact polyhedral subsets of $\mathcal{Y}$ converging towards $\mathcal{G}$ with respect to the Hausdorff distance (see Figure 1). The next step is the evaluation of the convergence of the minimizers of a sequence of problems in the form (2.1). A first important remark concerns the relation of the admissible sets in two different problems, when the corresponding sets of parameters are nested one into the other.

LEMMA 2.5. *Let us consider two subsets $\mathcal{G}_1$, $\mathcal{G}_2$ of a Banach space $\mathcal{Y}$ such that $\mathcal{G}_1 \subset \mathcal{G}_2$. We denote by E_1, E_2 the subsets of $\mathcal{S}_{\text{adm}} \subset \mathcal{D}_\varepsilon(\mathcal{B})$ where the inequality constraint of problem* (2.1) *is satisfied for the sets of parameters $\mathcal{G}_1$ and $\mathcal{G}_2$, respectively:*

$$E_i = \left\{ \Omega \in \mathcal{S}_{\text{adm}} \ : \ \sup_{\mathbf{g} \in \mathcal{G}_i} h(\mathbf{g}, \Omega) \leq \tau \right\} \qquad \text{for } i \in \{1, 2\}.$$

Then $E_2 \subset E_1$.

Proof. Let us consider $\Omega \in E_2$. Since all $\mathbf{g}_1 \in \mathcal{G}_1$ belongs also to $\mathcal{G}_2$, we have that $h(\mathbf{g}_1, \Omega) \leq \tau$ for all $\mathbf{g}_1 \in \mathcal{G}_1$. Thus $\Omega \in E_1$. ∎

Thanks to Lemma 2.5, we can prove the following result about the convergence of the solutions of a sequence of problems in the form (2.1).

PROPOSITION 2.6. *We consider $\{\mathcal{G}_n\}_{n=1}^{\infty}$ to be an increasing sequence of compact subsets of $\mathcal{Y}$ where $\mathcal{G}_i \subset \mathcal{G}_j$ if $i < j$ and such that $\mathcal{G} = \overline{\bigcup_{i=1}^{\infty} \mathcal{G}_i}$ is compact as well. Let $h : \mathcal{G} \times \mathcal{S}_{\text{adm}} \to \mathbb{R}$ be a function that satisfies assumptions* (i) *and* (ii)*, let $\mathcal{S}_{\text{adm}} \subset \mathcal{D}_\varepsilon(\mathcal{B})$ closed, and let $\tau \in \mathbb{R}$ be a given threshold. As in Lemma* 2.5*, we denote by E_i the subset of admissible domains $\mathcal{S}_{\text{adm}}$ such that if $\Omega \in E_i$, then $h(\mathbf{g}, \Omega) \leq \tau$ for all $g \in \mathcal{G}_i$. Finally, we denote by E the set of admissible domains such defined as*

$$E = \left\{ \Omega \in \mathcal{S}_{\text{adm}} \ : \ \sup_{\mathbf{g} \in \mathcal{G}} h(\mathbf{g}, \Omega) \leq \tau \right\},$$

and we suppose that neither any set E_i nor the set E is empty. Then the sequence $\{E_i\}_{i=1}^{\infty}$ is decreasing, in the sense that $E_i \supseteq E_j$ if $i < j$, $E = \bigcap_{i=1}^{\infty} E_i$, and E as well as all E_i are closed subsets of $\mathcal{S}_{\text{adm}}$ with respect to its metric m_{H}.

Proof. The fact that $\{E_i\}_{i=1}^{\infty}$ is a decreasing sequence follows from Lemma 2.5. Next, we prove the identity $E = \bigcap_{i=1}^{\infty} E_i$. The inclusion $E \subset \bigcap_{i=1}^{\infty} E_i$ is, again, a direct consequence of Lemma 2.5 since, for all $i > 0$, we suppose that $\mathcal{G} \supseteq \mathcal{G}_i$. In

order to prove the converse inclusion, we suppose that $\Omega \in E_i$ for all $i > 0$. Since we defined the set $\mathcal{G}$ as $\mathcal{G} = \overline{\bigcup_{i=1}^{\infty} \mathcal{G}_i}$, for all $\mathbf{g} \in \mathcal{G}$, there exists a sequence $\{\mathbf{g}_i\}_{i=1}^{\infty}$ such that $\mathbf{g}_i \in \mathcal{G}_i$ for all $i > 0$, and $\mathbf{g}_i \to \mathbf{g}$. By hypothesis, $\mathbf{g} \mapsto h(\mathbf{g}, \Omega)$ is convex on the finite-dimensional space $\mathcal{Y}$ and it is bounded. Thus, such mapping is also continuous (see [45, Corollary 10.1.1]). By the definition of the sets $\{E_i\}_{i=1}^{\infty}$ and the sequence $\{\mathbf{g}_i\}_{i=1}^{\infty}$, and by the continuity of $\mathbf{g} \mapsto h(\mathbf{g}, \Omega)$, we deduce that $h(\mathbf{g}, \Omega) \leq \tau$, and we conclude that $\Omega \in E$.

Let $i \in \mathbb{N}$. In order to prove that E_i is a closed set, we consider the function $\Phi_i : \mathcal{S}_{\text{adm}} \to \mathbb{R}^+$, mapping $\Omega \mapsto \sup_{\mathbf{g} \in \mathcal{G}_i} h(\mathbf{g}, \Omega)$. Such a function is well-defined and continuous on $\mathcal{S}_{\text{adm}}$, since the set of parameters $\mathcal{G}_i$ is compact. Thus, we deduce that $E_i = \Phi_i^{-1}([0, \tau])$ is a closed subset of $\mathcal{S}_{\text{adm}}$. Since $E = \bigcap_{i=1}^{\infty} E_i$, we conclude that E is closed with respect to the Hausdorff metric in $\mathcal{S}_{\text{adm}}$ as well. ∎

Now, we can state the main result of this section, which is about the convergence of the solution of a sequence of shape optimization problems in the form (2.4) with an increasingly accurate approximation of the set $\mathcal{G}$.

THEOREM 2.7. *We consider a compact set $\mathcal{B} \subset \mathbb{R}^d$, and a family of open domains $\mathcal{S}_{\text{adm}}$, uniformly bounded by $\mathcal{B}$ and closed in $\mathcal{D}_\varepsilon(\mathcal{B})$. Let $h : \mathcal{G} \times \mathcal{S}_{\text{adm}} \to \mathbb{R}$ be a function fulfilling assumptions* (i) *and* (ii)*, let $\tau \in \mathbb{R}$ be a given threshold, and let $\{\mathcal{G}_n\}_{n=1}^{\infty}$ be a sequence of compact subsets of $\mathcal{Y}$ satisfying the hypotheses of Proposition* 2.6*. Let $\{\Omega_i\}_{i=1}^{\infty}$ be a sequence of domains such that $\Omega_i \in \arg\min_{\Omega \in E_i} \text{Vol}(\Omega)$ for all $i \in \mathbb{N}$. Then $\{\Omega_i\}_{i=1}^{\infty}$ admits a converging subsequence with respect to the Hausdorff metric, and any Ω_∞ in the limit class is a solution of problem* (2.1).

Proof. Let us consider a sequence $\{\Omega_i\}_{i=1}^{\infty}$ such that $\Omega_i \in E_i$ for all $n > 0$. All sets E_i are closed subsets of $\mathcal{S}_{\text{adm}} \subset \mathcal{D}_\varepsilon(\mathcal{B})$ embedded into one another, and $\mathcal{D}_\varepsilon(\mathcal{B})$ is sequentially compact with respect to the Hausdorff metric [39, Theorem 2.4.10]. Thus, $\{\Omega_i\}_{i=1}^{\infty}$ admits a subsequence converging towards $\Omega_\infty \in \mathcal{D}_\varepsilon(\mathcal{B})$, and $\Omega_\infty \in E_i$ for all $i \in \mathbb{N}$. Thanks to Proposition 2.6 we deduce that $\Omega_\infty \in E$.

Finally, in order to prove that $\Omega_\infty \in \arg\min_{\Omega \in E} \text{Vol}(\Omega)$, we reason by contradiction. Let $\varepsilon > 0$ and $\Omega_\varepsilon \in E$ such that $\text{Vol}(\Omega_\infty) = \text{Vol}(\Omega_\varepsilon) + \varepsilon$. Since $\text{Vol}(\cdot)$ is a continuous function with respect to the metric m_{H}, there exists $N_\varepsilon > 0$ such that, for all $n > N_\varepsilon$, $\text{Vol}(\Omega_n) > \text{Vol}(\Omega_\varepsilon) + \varepsilon/2$. This result is in contradiction with the assumption $\Omega_n \in \arg\min_{\Omega \in E_n} \text{Vol}(\Omega)$, since $\Omega_\varepsilon \in E \subset E_n$. Therefore, we conclude that $\Omega_\infty \in \arg\min_{\Omega \in E} \text{Vol}(\Omega)$. ∎

One technique to solve problem (2.1) for a constraint functional $h(\cdot, \cdot)$ satisfying conditions (i) and (ii) consists in solving an approximate problem where the set of admissible parameters $\mathcal{G}$ is replaced by a convex polyhedral set $\mathcal{G}_N$ with N vertices. Theorem 2.7 suggests that, by increasing the accuracy of the approximation of $\mathcal{G}$ by $\mathcal{G}_N$, the solution of the approximate problem converges towards the solution of the original one. The approximate problems can then be solved as a simple constrained optimization problem using (2.2).

This approach suffers from two notable drawbacks. The first one is the fact that none of the polyhedral sets considered by Proposition 2.4 is a conservative approximation of the original set of admissible parameters $\mathbf{g}$. Therefore, for any approximation $\mathcal{G}_N$ of $\mathcal{G}$, denoting Ω_N the solution of the corresponding optimization problem, there exists a parameter $\widetilde{\mathbf{g}} \in (\mathcal{G} \setminus \mathcal{G}_N) \neq \emptyset$ such that $h(\widetilde{\mathbf{g}}, \Omega_N) > \tau$. A possible solution to this issue consists in considering a sequence of polyhedral sets converging towards $\mathcal{G}^*$ strictly containing $\mathcal{G}$. However, the convergence of the solutions of the approximated problems towards the solution of the original would be lost.

A second important issue from the numerical point of view concerns the number of points that are necessary to accurately approximate the finite-dimensional set $\mathcal{G}$. Indeed, as shown in [12], given a convex set $\mathcal{G} \subset \mathbb{R}^n$ of class $\mathcal{C}^2$ and a tolerance $\epsilon > 0$, the minimal number of vertices $N_{\mathcal{G},\epsilon}$ such that the Hausdorff distance between their convex hull and $\mathcal{G}$ is bounded by ϵ is

$$N_{\mathcal{G},\epsilon} \geq \left(\frac{c(\mathcal{G})}{\epsilon} \right)^{\frac{n-1}{2}}, \tag{2.3}$$

where $c(\mathcal{G})$ is a constant depending on the shape of the convex set. Equation (2.3) proves that the number of vertices that are necessary to approximate a given convex set for a given precision increases exponentially with respect to the dimension of the space of parameters. Since any vertex in the approximating polyhedron corresponds to a constraint in problem (2.1), an exponentially increasing number of constraints has to be evaluated for the solution of the optimization problem, indicating that this approach suffers from the curse of dimensionality.

3. An approach based on subdifferentials. Another approach to solving problem (1.2) by a gradient-based method consists in differentiating directly the constraint function $\Omega \mapsto \sup_{\mathbf{g}\in\mathcal{G}} H(\mathbf{u}_{\Omega,\mathbf{g}}, \Omega)$. The question of the derivative with respect to the domain of nondifferentiable shape functionals has been considered in the literature from different points of view. The authors of [43, 2] are interested in the optimization with respect to nonsmooth functionals. In [5, 24, 17, 16], the quantity of interest consists in the first eigenvalue of different functionals, which can be expressed as minima of suitable Rayleigh quotients. In particular, the approach proposed in [17, 16] consists in the computation of a semiderivative in the sense of Danskin [27] by applying a result from Delfour and Zolésio [32, Theorem 2.1, Chapter 10] on the sensitivity of a minimum with respect to a parameter. In this section, we present an approach inspired by the methods of [37], relying on the notion of subdifferentiability of nonsmooth functions as introduced by Clarke in [21]. The main tool we use in this work is a result presented as [21, Corollary 2 of Theorem 2.8.2] and referenced in [37, section 4.2].

3.1. Generalized shape derivative of a maximum of a family of objectives. Similarly to what has been done in subsection 2.2, we consider a generic optimization problem without an explicit expression of the state-like problem (2.1). For the sake of simplicity, we denote by $\Phi : \mathcal{S}_{\mathrm{adm}} \to \mathbb{R}$ the shape functional defined as

$$\Phi(\Omega) = \sup_{\mathbf{g}\in\mathcal{G}} h(\mathbf{g}, \Omega). \tag{3.1}$$

Unfortunately, [21, Corollary 2 of Theorem 2.8.2] cannot be directly applied to differentiate Φ, since the space $\mathcal{S}_{\mathrm{adm}}$ provided with the Hausdorff metric m_{H} is not a Banach space. Such an issue can be bypassed thanks to the definition of the shape derivative according to Hadamard. Indeed, for a given admissible domain $\Omega \in \mathcal{S}_{\mathrm{adm}}$, the deformation field $\boldsymbol{\theta}$ at the core of Hadamard's moving boundaries approach belongs to the Banach space $\mathrm{W}^{1,\infty}(\mathbb{R}^d)^d$. With this in mind, we can extend the concepts of subdifferential to shape functionals.

DEFINITION 3.1 (subdifferential of a shape functional). *Let $\Omega \in \mathcal{S}_{\mathrm{adm}}$ be a domain in $\mathbb{R}^d$, and let $J : \mathcal{S}_{\mathrm{adm}} \to \mathbb{R}$ be a shape functional such that the mapping $\boldsymbol{\theta} \mapsto J(\Omega_{\boldsymbol{\theta}})$ admits a Gâteaux derivative $\mathrm{d}J(\Omega;\boldsymbol{\theta})$ for all $\boldsymbol{\theta} \in \mathrm{W}^{1,\infty}(\mathbb{R}^d)^d$. Then the subdifferential of J in Ω is defined as*

$$\partial J(\Omega) = \left\{ L \in \left(\mathrm{W}^{1,\infty}\left(\mathbb{R}^d\right)^d \right)^* \,:\, \mathrm{d}J(\Omega;\boldsymbol{\theta}) \geq L(\boldsymbol{\theta}) \text{ for all } \boldsymbol{\theta} \in \mathrm{W}^{1,\infty}\left(\mathbb{R}^d\right)^d \right\}.$$

We can now state a result for the differentiation of the maximum of a family of shape functionals. It is an almost direct application of the general Clarke's result presented as [21, Corollary 2 of Theorem 2.8.2] and referred to and already used, for example, in [37, section 4.2].

PROPOSITION 3.2. *Let $\mathcal{S}_{\mathrm{adm}}$ be a family of uniformly bounded open domains in $\mathbb{R}^d$ endowed with the topology induced by the Hausdorff metric m_{H}, and let $\mathcal{G}$ be a compact subset of a Banach space $(\mathcal{Y}, \|\cdot\|)$. Let $\Omega \in \mathcal{S}_{\mathrm{adm}}$ be an admissible domain, and let $h : \mathcal{G} \times \mathcal{S}_{\mathrm{adm}} \to \mathbb{R}$ be a shape functional such that*

(SA1) *$\widetilde{\Omega} \mapsto h(\mathbf{g}, \widetilde{\Omega})$ is Lipschitz continuous in a neighborhood U_Ω of Ω for any choice of the parameter $\mathbf{g} \in \mathcal{G}$;*

(SA2) *$\mathbf{g} \mapsto h(\mathbf{g}, \widetilde{\Omega}) \mathbf{g} \mapsto h(\mathbf{g}, \widetilde{\Omega})$ is convex and bounded for all $\widetilde{\Omega} \in U_\Omega$;*

(SA3) *$\widetilde{\Omega} \mapsto h(\mathbf{g}, \widetilde{\Omega})$ is Fréchet differentiable in U_Ω for any $\mathbf{g} \in \mathcal{G}$;*

(SA4) *the Fréchet derivative $\frac{\partial h}{\partial \Omega}(\mathbf{g}, \widetilde{\Omega}) \in (\mathrm{W}^{1,\infty}(\mathbb{R}^d)^d)^*$ is continuous in $\mathcal{G} \times U_\Omega$.*

We denote by $\Phi : \mathcal{S}_{\mathrm{adm}} \to \mathbb{R}$ the shape functional

$$\Omega \mapsto \Phi(\Omega) = \max_{\mathbf{g} \in \mathcal{G}} h(\mathbf{g}, \Omega),$$

where the maximum is attained thanks to the convexity of $h(\cdot, \mathbf{g})$ and compactness of $\mathcal{G}$. Then the functional $\Phi(\cdot)$ admits a subdifferential $\partial\Phi(\Omega)$ in Ω, and its expression is given by

$$\partial\Phi(\Omega) = \left\{ \int_{\mathcal{G}} \frac{\partial h}{\partial \Omega}(\mathbf{g}, \Omega)\, \mathrm{d}\mu(\mathbf{g}) \,:\, \mu \in P[\mathcal{G}(\Omega)] \right\} \subset \left(\mathrm{W}^{1,\infty}\left(\mathbb{R}^d\right)^d \right)^*.$$

Proof. We consider the class $\Theta_\Omega \subset \mathrm{W}^{1,\infty}(\mathbb{R}^d)^d$ of admissible deformations defined as

$$\Theta_\Omega = \left\{ \boldsymbol{\theta} \in \mathrm{W}^{1,\infty}\left(\mathbb{R}^d\right)^d \,:\, \Omega_{\boldsymbol{\theta}} \in U_\Omega \right\}.$$

We introduce the function $f_\Omega : \mathcal{G} \times \Theta_\Omega \to \mathbb{R}$ mapping $(\mathbf{g}, \boldsymbol{\theta}) \mapsto f_\Omega(\mathbf{g}, \boldsymbol{\theta}) = h(\mathbf{g}, \Omega_{\boldsymbol{\theta}})$. In order to prove Proposition 3.2, we verify that f_Ω satisfies all the hypotheses of [21, Corollary 2 of Theorem 2.8.2]. At first, we observe that the set $\mathcal{G}$ is compatible with the hypotheses of Clarke's theorem [21, Corollary 2 of Theorem 2.8.2], since it is a compact subset of the Banach space $\mathcal{Y}$ with respect to the Hausdorff metric m_{H}. The set Θ_Ω is a neighborhood of the origin in the Banach space $\mathrm{W}^{1,\infty}(\mathbb{R}^d)^d$.

The continuity of $f_\Omega(\cdot, \boldsymbol{\theta})$ for all $\boldsymbol{\theta} \in \Theta_\Omega$ is ensured by the convexity of $\mathbf{g} \mapsto h(\mathbf{g}, \widetilde{\Omega})$ for all $\widetilde{\Omega} \in U_\Omega$. The existence and continuity of the strict derivative of $\boldsymbol{\theta} \mapsto f_\Omega(\mathbf{g}, \boldsymbol{\theta})$ follow from assumptions (SA3) and (SA4). Therefore, the function $\boldsymbol{\theta} \mapsto F_\Omega(\boldsymbol{\theta}) = \max_{\mathbf{g} \in \mathcal{G}} f_\Omega(\mathbf{g}, \boldsymbol{\theta})$ is well defined, and it admits a subdifferential $\partial F_\Omega(\boldsymbol{\theta})$ with the following expression:

$$\partial F_\Omega(\boldsymbol{\theta}) = \left\{ \int_{\mathcal{G}} \frac{\partial f_\Omega}{\partial \boldsymbol{\theta}}(\mathbf{g}, \boldsymbol{\theta})\, \mathrm{d}\mu(\mathbf{g}) \,:\, \mu \in P[\mathcal{G}(\Omega)] \right\} \subset \left(\mathrm{W}^{1,\infty}\left(\mathbb{R}^d\right)^d \right)^*.$$

Thanks to the definitions of the functionals Φ and F_Ω we have that, for all $\boldsymbol{\theta} \in \Theta_\Omega$, $\Phi(\Omega_{\boldsymbol{\theta}}) = F_\Omega(\boldsymbol{\theta})$ and, in particular, $\Phi(\Omega) = F_\Omega(\mathbf{0})$. Thus, $\partial\Phi(\Omega) = \partial F_\Omega(\mathbf{0})$. ∎

Proposition 3.2 provides a method to compute elements of the subdifferential according to the shape $\partial\Phi(\Omega)$ by computing a value of the parameter $\mathbf{g} \in \mathcal{G}$, where

$h(\Omega, \mathbf{g})$ attains its maximum. Differently from the case studied in section 2, the convexity of the set $\mathcal{G}$ of external loads is not required. It should also be remarked that any element of the subdifferential defines a direction of descent for the functional Φ, albeit not necessarily optimal if $\partial\Phi(\Omega)$ is not a singleton.

Remark. In the introduction, we did not assume that f is in $\mathrm{H}^{-1}(\Omega)$ and g in $\mathrm{H}^{-1/2}(\Gamma_N)$, which would be the natural spaces. If the shape derivative is well defined in these spaces, we need to write down its expression in order to calculate it numerically. An additional derivative of the state function appears, and the solution to the equation of state must be more regular to make sense of this expression. It is for this technical reason that we have assumed this additional unexpected regularity.

3.2. Algorithmic implementation. Let us consider the same notation of Proposition 3.2: $\mathcal{G}$ is a compact subset of a Banach space $(\mathcal{Y}, \|\cdot\|)$, $h : \mathcal{G} \times \mathcal{S}_{\mathrm{adm}} \to \mathbb{R}$ is a function satisfying the conditions (SA1)–(SA4) of Proposition 3.2, and $\Phi(\cdot)$ is the shape functional mapping $\Omega \mapsto \max_{\mathbf{g}\in\mathcal{G}} h(\mathbf{g}, \Omega)$.

In subsection 3.1 we provided the theoretical framework for the computation of the subdifferential of $\Phi(\cdot)$. Here we provide a procedure to compute one element to the subdifferential $\partial\Phi(\Omega)$. The procedure can be divided into two steps. First, we identify a parameter $\overline{\mathbf{g}} \in \arg\max_{\mathbf{g}\in\mathcal{G}} h(\mathbf{g}, \Omega) \subset \mathcal{G}$ for which the maximum of $h(\cdot, \Omega)$ is attained. The maximum is attained in at least one point, since $\mathcal{G}$ is compact, and $h(\cdot, \Omega)$ is convex and bounded (see Proposition 2.1). Next, the shape derivative of the term $h(\overline{\mathbf{g}}, \Omega)$ is computed using the classical methods of boundary variation. Proposition 3.2 ensures that the shape derivative of $h(\overline{\mathbf{g}}, \Omega)$ belongs to the subdifferential $\partial\Phi(\Omega)$.

Different possible methods can be considered to identify the parameter $\overline{\mathbf{g}}$ depending on the nature of the set $\mathcal{G}$ and the function $h(\cdot, \Omega)$. If the mapping $\mathbf{g} \mapsto h(\mathbf{g}, \Omega)$ is differentiable with respect to $\mathbf{g}$ and $\mathcal{G}$ is a subset of a Hilbert space, a simple gradient-descent method can be implemented to identify $\overline{\mathbf{g}}$. If further hypotheses apply on the constraint functional or on the set of admissible parameters, ad hoc methods can be used. An example for the case where $\mathbf{g} \mapsto h(\mathbf{g}, \Omega)$ is a quadratic function and $\mathcal{G}$ an ellipsoid is provided in subsection 4.3.

4. Numerical results.

4.1. Numerical implementation. For both approaches, we performed the numerical simulations using the platform provided by Dapogny and Feppon in [29], coupling the *nullspace optimization* algorithm [34] with the PDE solver *FreeFem++* using the finite elements method [38], the simplicial remeshing software *mmg* [28, 11], and the programs *advect* [15] and *mshdist* [30] from the *ISCD toolbox.*

At each iteration of the optimization algorithm, the shape Ω is encoded by a level-set function defined over a tetrahedral mesh on a fixed computational domain. The implicit domain meshing functionality of *mmg* is employed in order to extract an explicit mesh for Ω. The solver *FreeFem++* is used to compute the quantity of interests as the displacements, the volume of the structure, and the concentration of the von Mises stress, as well as the shape derivative and gradients of the objective and the constraints of the optimization problem.

Finally, the advection equation for the level-set function is solved by the *advect* program and regularized by *mshdist* into a level set for the deformed domain which is a signed-distance function. For more details on the numerical implementation, we refer the reader to the article about the general numerical framework [29].

The nullspace algorithm introduced by Feppon, Allaire, and Dapogny in [34] has become popular in numerical shape optimization. This optimization algorithm starts

from a point that does not satisfy the constraint and seeks to orient itself in such a way as to first satisfy the constraint while reducing the objective if possible. Interested readers are referred to the article [34] for a precise definition of the algorithm and a study of its properties. Its main advantage is to be able to deal with numerous constraints, and this motivates our choice since we wanted to be able to deal with additional constraints imposed by engineers like minimal width–type constraints (see [6]).

In the case of the method based on the subdifferential, we use a basic method by retaining only one element of the subdifferential obtained by calculating a single loading that maximizes the criterion. We are well aware that this is a possible point of improvement by using more complex dedicated methods as presented, for example, in [40].

The simulations of this section have been executed on a Virtualbox virtual machine Linux with 1 GB of dedicated memory, installed on a Dell PC equipped with a 2.80 GHz Intel i7 processor.

4.2. Disc. As an initial numerical application, we consider the optimization of a cylinder-like structure, aiming to minimize its volume under a constraint on the L^6-norm of the von Mises stress. Thus, the constraint functional is defined as

$$\|s_{\mathrm{D}}(\mathbf{u}_\Omega)\|_6 = \sqrt{\frac{3}{2}}\left(\int_\Omega \left(\boldsymbol{\sigma}_{\mathrm{D}}(\mathbf{u}_\Omega) : \boldsymbol{\sigma}_{\mathrm{D}}(\mathbf{u}_\Omega)\right)^3 \mathrm{d}\mathbf{x}\right)^{1/6}, \tag{4.1}$$

where $\boldsymbol{\sigma}_{\mathrm{D}}(\mathbf{u}_\Omega) = \boldsymbol{\sigma}(\mathbf{u}_\Omega) - \frac{1}{3}\mathbb{I}\,\mathrm{tr}(\boldsymbol{\sigma}(\mathbf{u}_\Omega))$ is the deviatoric part of the stress tensor. Refer to [10, 41] for more information on the physical interpretation of von Mises stress.

The initial condition is presented in Figure 2: the structure is fixed on a region Γ_{D} on its side, while shear loads are applied tangentially to a ring-like surface Γ_{N} on the top of the cylinder. The optimization problem to be solved is the following:

$$\left|\begin{array}{l} \text{Find the admissible shape } \Omega \in \mathcal{S}_{\mathrm{adm}} \text{ minimizing the volume } \mathrm{Vol}(\Omega) \\ \text{under the constraint } \sup_{\mathbf{g}\in\mathcal{G}} \|s_{\mathrm{D}}(\mathbf{u}_\Omega)\|_6 \le \tau, \\ \text{where the displacement } \mathbf{u}_{\Omega,\mathbf{g}} \text{ solves (1.1).} \end{array}\right. \tag{4.2}$$

We suppose that the load $\mathbf{g}$ can be written as the sum of two terms, tangent to the upper surface of the structure and aligned with the axes x and y:

$$\mathbf{g} = X\mathbf{e}_x + Y\mathbf{e}_y.$$

FIG. 2. *Structure of the 3D disc structure. The region Γ_{N} where the random load is applied is marked in red, while the clamping region Γ_{D} is highlighted in gray. (Color available online.)*

We consider that the intensity of the applied force is bounded by $\overline{g}$, so that the set of admissible loads $\mathcal{G}$ can be parameterized by a circle in $\mathbb{R}^2$ with radius $\overline{g}$. The geometric and material properties of the structure, the mesh size, the maximal value of the applied force, and the threshold τ on the L^6-norm of the von Mises stress are reported in Table 4 in the appendix.

We consider three different approximations for the polyhedral approach, where $\mathcal{G}$ is replaced by inscribed regular polygons with $N = 4$, 8, and 16 vertices denoted $\mathcal{G}_4$, $\mathcal{G}_8$, and $\mathcal{G}_{16}$, respectively. These polygons can thus be defined as convex hulls of N points as follows:

$$\mathcal{G}_N = \text{hull}\left\{\overline{g}\left(\sin\left(\frac{2n\pi}{N}\right)\mathbf{e}_x + \cos\left(\frac{2n\pi}{N}\right)\mathbf{e}_y\right) \ : \ n \in \{0,\dots,N-1\}\right\} \subset \mathbb{R}^2.$$

Thanks to the symmetry of the constraint with respect to a change of sign in the applied force (and thus in the displacement $\mathbf{u}_{\Omega,\mathbf{g}}$), only $N/2$ constraints need to be evaluated at each step of the solution of problem (4.2). The structures resulting from applying the polyhedral approximation method are shown in Figure 3c and denoted as Ω_4, Ω_8, and Ω_{16}, respectively.

We remark that the increasing refinement in the approximation of $\mathcal{G}$ results in structures that differ significantly from one another. Indeed, we can see how Ω_4 (Figure 3a) is optimized to resist the forces applied in the directions of the four edges of $\mathcal{G}_4$. The structure Ω_8 (Figure 3b) with eight scenarios is similar, but its four branches are wider, responding to forces oriented in the direction bisecting the main axes. Finally, Ω_{16} (Figure 3c) is characterized by a rotational symmetry, thus resisting to forces applied in 16 different directions.

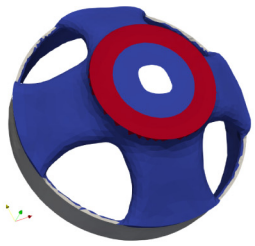

(a) Polyhedron approach, $N = 4$.

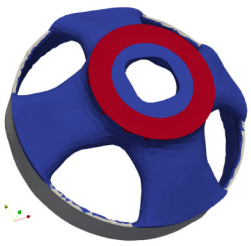

(b) Polyhedron approach, $N = 8$.

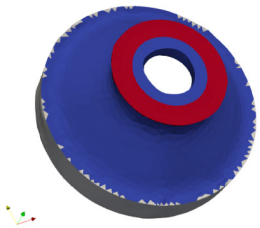

(c) Polyhedron approach, $N = 16$.

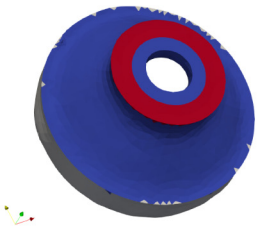

(d) Subdifferential approach.

FIG. 3. *Optimal shape of the disc structure for the polyhedron and subdifferential approaches.*

TABLE 1

Numerical results for the optimization of the volume of a disc structure under constraints on the L^6-norm of the von Mises stress, obtained using the polyhedron method (with an increasing number of vertices) and the subdifferential method.

		Polyhedron			
		$N=4$	$N=8$	$N=16$	**Subdifferential**
Execution of the optimization					
Duration of the optimization	[min]	189	296	499	159
Number of iterations		200	200	200	300
Results					
Final volume Vol(Ω)	[cm^3]	666.27	692.18	751.46	874.07
Maximal von Mises stresses	[kPa]	5.015	5.053	5.164	5.183
$d_H(\Omega_S, \Omega_N)$	[cm]	3.001	3.037	1.347	–

Let us denote by $\overline{\mathbf{g}}$ the element of $\mathcal{G}$ maximizing the constraint functional. By the convexity of the mapping $\mathbf{g} \mapsto \|s_D(\mathbf{u}_\Omega)\|_6$ Proposition 2.1 applies, and we deduce that $\overline{\mathbf{g}}$ belongs to the boundary of $\mathcal{G}$. Thus, there exist $\alpha \in [0, 2\pi)$ such that

$$\overline{\mathbf{g}} = \overline{g}\,(\sin\alpha\,\mathbf{e}_x + \cos\alpha\,\mathbf{e}_y)\,.$$

The constraint functional considered in problem (4.2) is the L^6-norm of the von Mises stress, which is not a quadratic function. We identify the value of α maximizing the constraint function by applying the Newton method to the function $\alpha \mapsto (\|s_D(\mathbf{u}_\Omega)\|_6)^6$. It should be remarked that such a function can be expressed analytically in terms of the displacement fields generated by the application of the loads $\overline{g}\mathbf{e}_x$ and $\overline{g}\mathbf{e}_y$. Thus its evaluation is extremely fast and does not require the solution of an expensive boundary value problem. Thanks to the symmetry of the constraint under a change of sign of the mechanical load, the search of the critical direction α can be limited to the interval $[-\frac{\pi}{2}, \frac{\pi}{2})$. The shape Ω_S resulting from the application of the subdifferential approach is reported in Figure 3d.

The numerical results of the optimization performed using the polyhedral approximation and the subdifferential method are reported in Table 1. In Figure 4 are plotted the value of the maximal constraint throughout the optimization: first for the three instances of the polyhedral approximation algorithm (Figure 4a), and then comparing them with the evolution of the constraints for the subdifferential approach (Figure 4b). The trend of the objective function for all four simulations is represented in Figure 5a. In Figure 5b we report the evolution of the angle α parametrizing the direction of the load maximizing the L^6-norm of the von Mises stress at each step.

The method of subdifferential yields an optimal structure Ω_S with rotational symmetry similar to the most precise polyhedral approximation Ω_{16}, as shown by Figure 3d. If we assume that Ω_S is representative of the exact solution of problem (4.2), the comparison of the illustrations of the optimal shapes validates the convergence result of Theorem 2.7. Indeed, the similarity between Ω_N and Ω_S increases when $\mathcal{G}_N$ better approximates the original set $\mathcal{G}$. This statement is corroborated by the numerical computation of the Hausdorff distances between Ω_S and the shapes resulting from the polyhedral approximation, as shown in Table 1.

A first remark concerns the overall convergence of the optimization algorithm for the different approaches. Indeed the value of the constraint functional appears to deviate from the threshold for extended intervals of time, as shown in the two parts of Figure 4. In Figure 5a, similar deviations from the downward trend of the objective function can be observed for all three applications of the polyhedral approximation.

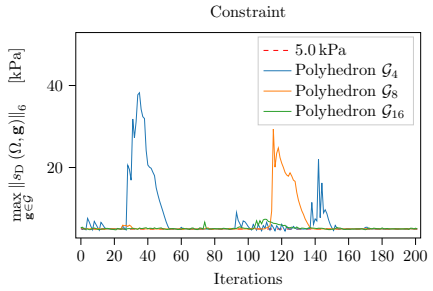

(a) Evolution of the constraint for three instances of the polyhedron method (4, 8, and 16 vertices, respectively).

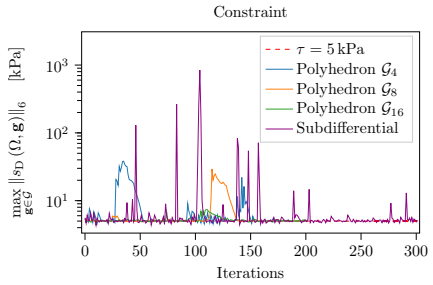

(b) Evolution of the constraint for three instances of the polyhedron method, and the subdifferential method.

FIG. 4. *Convergence of the constraint (L^6-norm of the von Mises stress) for the disc structure.*

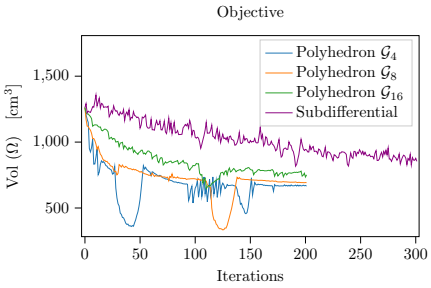

(a) Evolution of the objective function.

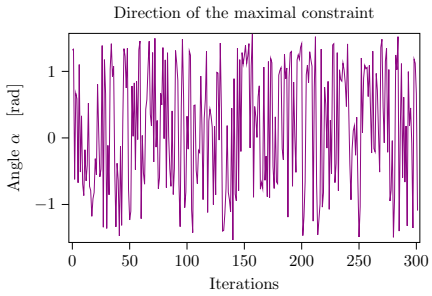

(b) Evolution of the direction of the maximal constraint (in terms of the angle α) during the optimization process.

FIG. 5. *Convergence of the objective (volume) for the polyhedron and subdifferential methods, and direction of the largest constraint under the subdifferential method for the disc structure.*

Such perturbations are due to the larger sensitivity of the L^6-norm of the von Mises stress with respect to small perturbations of the shape, compared to the sensitivity of the mechanical compliance.

By looking at the graph of Figure 4b we remark that the constraint on the maximum of the L^6-norm of the von Mises stress is overall satisfied by the method of subdifferential, but more significant perturbations can be observed. A more difficult convergence compared to the polyhedron method can be remarked in Figure 5a, where a slower decrease in the objective function is evident, to the point that a larger number of iterations has been necessary in order to reach a stable configuration (200 for the polyhedron method and 300 for the subdifferential). Both issues are justified by the rotational symmetry of the optimization problem. As the graph in Figure 5b shows, the critical direction α varies widely at each step of the optimization algorithm, even from one iteration to the next. This entails that a deformation of the shape aiming to strengthen the structure with respect to stresses in a certain direction might weaken it for stresses applied in different directions. Thus, a larger number of smaller optimization steps is necessary in order to ensure that the structure remains capable of resisting stresses in all directions throughout the optimization process.

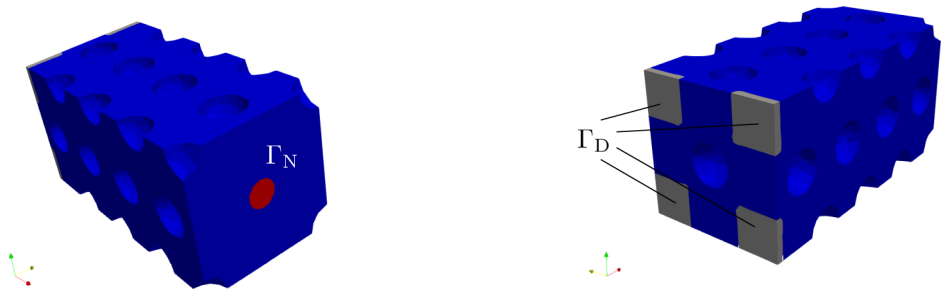

FIG. 6. *Structure of the 3D cantilever structure. The region Γ_N where the uncertain mechanical load is applied is marked in red, while the clamping region Γ_D is highlighted in gray. (Color available online.)*

By comparing the duration of the simulations as presented in Table 1, we observe that the subdifferential approach is overall faster than the polyhedral approximation, since it requires fewer evaluations of the constraint functional. Therefore, the shorter duration of each step compensates for the smaller contribution of each iteration to the decrease of the objective function.

4.3. 3D Cantilever. In this section, we consider the optimization of a 3D cantilever structure under a constraint on the mechanical compliance given by

$$\mathcal{C}\left(\mathbf{u}_{\Omega,\mathbf{g}},\Omega\right)=\int_{\Omega}\mathbf{f}\cdot\mathbf{u}_{\Omega,\mathbf{g}}\,\mathrm{d}\mathbf{x}+\int_{\Gamma_N}\mathbf{g}\cdot\mathbf{u}_{\Omega,\mathbf{g}}\,\mathrm{d}\mathbf{s}.$$

Then we consider the following problem:

$$\left|\begin{array}{l}\text{Find the admissible shape } \Omega\in\mathcal{S}_{\mathrm{adm}} \text{ minimizing the volume } \mathrm{Vol}(\Omega)\\ \text{under the constraint } \sup_{\mathbf{g}\in\mathcal{G}}\mathcal{C}\left(\mathbf{u}_{\Omega,\mathbf{g}},\Omega\right)\leq\tau,\\ \text{where the displacement } \mathbf{u}_{\Omega,\mathbf{g}}\in\mathrm{H}^1_{\Gamma_D}(\Omega)^d \text{ solves (1.1).}\end{array}\right. \tag{4.3}$$

The initial condition of the structure is presented in Figure 6: the structure is clamped on the four corners marked Γ_D, and the mechanical load $\mathbf{g}$ is applied on the region Γ_N on the opposite side. We suppose that the load $\mathbf{g}$ applied to Γ_N consists of two components: one of traction-compression (oriented along the x axis), and a vertical one (along the z axis):

$$\mathbf{g}=X\mathbf{e}_x+Z\mathbf{e}_z. \tag{4.4}$$

We suppose also that X and Z belong to the intervals $[-\overline{g}_x,\overline{g}_x]$ and $[-\overline{g}_z,\overline{g}_z]$, respectively. Moreover, we suppose that they are bounded by the inequality

$$\frac{X^2}{\overline{g}_x^2}+\frac{Z^2}{\overline{g}_z^2}\leq 1. \tag{4.5}$$

Inequality (4.5) states that the set of admissible mechanical loads can be parameterized by an ellipse in $\mathbb{R}^2$ with semiaxes equal to $\overline{g}_x$ and $\overline{g}_z$.

The numerical parameters considered for this problem are reported in Table 5 in the appendix.

In order to solve the optimization problem (4.3) we consider both the polyhedral approximation approach of section 2 and the method based on the subdifferential as

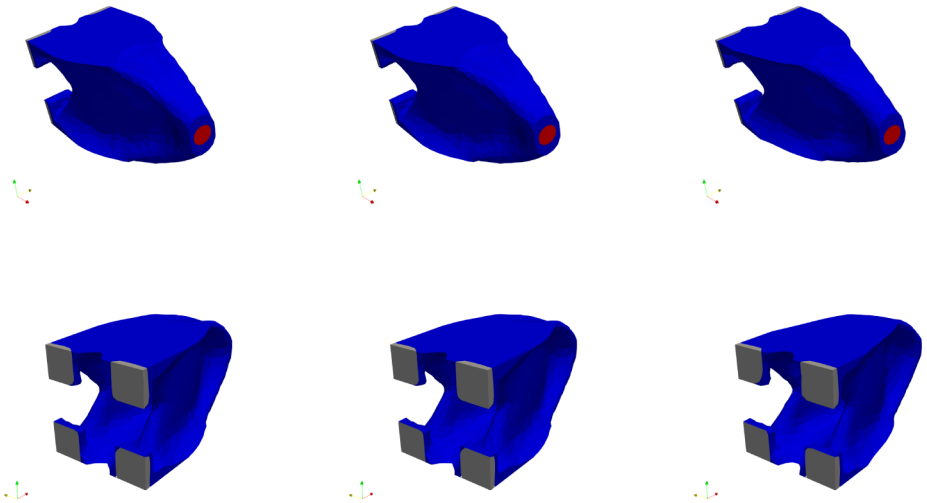

FIG. 7. *Optimal shapes for the polyhedron approach with* $N = 4, 8, 16$ *vertices (left to right).*

in section 3. Both methods can be applied since the set $\mathcal{G}$ is convex, the mapping $\mathbf{g} \mapsto \mathcal{C}(\mathbf{u}_{\Omega,\mathbf{g}}, \Omega)$ is a convex function, and the compliance operator satisfies conditions (SA1)–(SA4) of Proposition 3.2.

For the polyhedral approach, we approximated the ellipse $\mathcal{G}$ by polygons with 4, 8, and 16 vertices denoted $\mathcal{G}_4$, $\mathcal{G}_8$, and $\mathcal{G}_{16}$, respectively. The polygons $\mathcal{G}_4$, $\mathcal{G}_8$, and $\mathcal{G}_{16}$ are defined as convex hulls of N points as follows:

$$\mathcal{G}_N = \operatorname{hull}\left\{ \left(\overline{g}_x \sin\left(\frac{2n\pi}{N}\right) \mathbf{e}_x + \overline{g}_z \cos\left(\frac{2n\pi}{N}\right) \mathbf{e}_y \right) \,:\, n \in \{0, \dots, N-1\} \right\} \subset \mathbb{R}^2.$$

It should be remarked that since the compliance is invariant with respect to a change of sign in the applied load, it is necessary to consider only half of the vertices of $\mathcal{G}_4$, $\mathcal{G}_8$, and $\mathcal{G}_{16}$ to define the constraints of the approximated optimization problem. The structures optimized for the three cases are denoted Ω_4, Ω_8, and Ω_{16}, respectively. As shown in Figure 7, the optimal shapes for the three cases are extremely similar to one another.

In the subdifferential approach, it is necessary to identify the parameter $\overline{\mathbf{g}}$ maximizing $\mathcal{C}(\cdot, \Omega)$ at each step of the optimization. We can assume, by Proposition 2.1, that $\overline{\mathbf{g}}$ belongs to the boundary of $\mathcal{G}$. Therefore, there exists an angle $\alpha \in [0, 2\pi)$ such that

$$\overline{\mathbf{g}} = \sin\alpha\, g_x \mathbf{e}_x + \cos\alpha\, g_z \mathbf{e}_z.$$

Thanks to the symmetry of the compliance operator, we can restrict the search for α to the interval $[-\frac{\pi}{2}, \frac{\pi}{2})$. The angle α yielding the maximal compliance for a given shape Ω can be identified by interpreting the compliance as a quadratic functional. Indeed, there exists a matrix $\mathbf{M}_\Omega \in \mathbb{R}^{2\times 2}$ such that, for all $\hat{\alpha} \in [0, 2\pi)$,

$$\mathcal{C}(\mathbf{u}_{\Omega,\mathbf{g}}, \Omega) = \left(\sin\hat{\alpha}, \cos\hat{\alpha}\right) \mathbf{M}_\Omega \begin{pmatrix} \sin\hat{\alpha} \\ \cos\hat{\alpha} \end{pmatrix}, \tag{4.6}$$

where the load associated to $\mathbf{u}_{\Omega,\mathbf{g}}$ is $\mathbf{g}(\hat{\alpha}) = \sin\hat{\alpha} g_x \mathbf{e}_x + \cos\hat{\alpha} g_z \mathbf{e}_z$. The entries of the matrix $\mathbf{M}_\Omega$ are

$$[\mathbf{M}_\Omega]_{11} = m_{11} = \int_\Omega \boldsymbol{\sigma}\left(\mathbf{u}_{\Omega,\mathbf{g}_x}\right) : \boldsymbol{\varepsilon}\left(\mathbf{u}_{\Omega,\mathbf{g}_x}\right) \mathrm{d}\mathbf{x},$$
$$[\mathbf{M}_\Omega]_{22} = m_{22} = \int_\Omega \boldsymbol{\sigma}\left(\mathbf{u}_{\Omega,\mathbf{g}_z}\right) : \boldsymbol{\varepsilon}\left(\mathbf{u}_{\Omega,\mathbf{g}_z}\right) \mathrm{d}\mathbf{x},$$
$$[\mathbf{M}_\Omega]_{12} = [\mathbf{M}_\Omega]_{21} = m_{12} = \int_\Omega \boldsymbol{\sigma}\left(\mathbf{u}_{\Omega,\mathbf{g}_x}\right) : \boldsymbol{\varepsilon}\left(\mathbf{u}_{\Omega,\mathbf{g}_z}\right) \mathrm{d}\mathbf{x}.$$

The angle α for which the maximum of the compliance is attained depends on the eigenvector related to the maximal eigenvalue of $\mathbf{M}_\Omega$. In particular, α can be computed explicitly by the following expression:

(4.7)
$$\alpha = \begin{cases} \dfrac{\pi}{4} - \dfrac{\beta}{2} & \text{if } m_{12} \geq 0, \\ \dfrac{3\pi}{4} + \dfrac{\beta}{2} & \text{if } m_{12} < 0, \end{cases} \qquad \text{where } \beta = \arcsin\left(\frac{m_{22} - m_{11}}{2\sqrt{\left(\frac{m_{22}-m_{11}}{2}\right)^2 + m_{12}^2}} \right).$$

The expression of the optimal angle α of (4.7) can be found by developing (4.6):

(4.8)
$$\mathcal{C}\left(\mathbf{u}_{\Omega,\mathbf{g}}, \Omega\right) = m_{11}\sin^2\hat{\alpha} + m_{22}\cos^2\hat{\alpha} + m_{12}\sin\hat{\alpha}\cos\hat{\alpha} = \frac{m_{11}+m_{22}}{2}$$
$$+ \frac{m_{22}-m_{11}}{2}\cos 2\hat{\alpha} + m_{12}\sin 2\hat{\alpha} = \frac{m_{11}+m_{22}}{2} + \frac{\sqrt{\left(m_{22}-m_{11}\right)^2 + 4m_{12}^2}}{2}$$
$$\times \left(\frac{(m_{22}-m_{11})\cos 2\hat{\alpha}}{\sqrt{\left(m_{22}-m_{11}\right)^2 + 4m_{12}^2}} + \frac{2m_{12}\sin 2\hat{\alpha}}{\sqrt{\left(m_{22}-m_{11}\right)^2 + 4m_{12}^2}} \right).$$

As it is defined in (4.7), the angle β belongs to the interval $(-\frac{\pi}{2}, \frac{\pi}{2}]$. If $m_{12} \geq 0$, the expression (4.8) can be written as

$$\mathcal{C}\left(\mathbf{u}_{\Omega,\mathbf{g}}, \Omega\right) = \frac{m_{11}+m_{22}}{2} + \frac{\sqrt{\left(m_{22}-m_{11}\right)^2 + 4m_{12}^2}}{2}\sin\left(\beta + 2\hat{\alpha}\right),$$

which is maximized for $\hat{\alpha} = \frac{\pi}{4} - \frac{\beta}{2}$. If, on the other hand, $m_{12} < 0$, the expression for the compliance becomes

$$\mathcal{C}\left(\mathbf{u}_{\Omega,\mathbf{g}}, \Omega\right) = \frac{m_{11}+m_{22}}{2} + \frac{\sqrt{\left(m_{22}-m_{11}\right)^2 + 4m_{12}^2}}{2}\sin\left(\beta - 2\hat{\alpha}\right),$$

attaining its maximum for $\hat{\alpha} = \frac{3\pi}{4} + \frac{\beta}{2}$.

The optimal shape resulting from the optimization based on the subdifferential is reported in Figure 8, and we denote it by Ω_S. In the graph of Figure 9 is reported the evolution of the angle α along the iterations. We remark that α oscillates around 0, underscoring the fact that vertical loads which are orthogonal to the main axis of the cantilever are responsible for the largest values of the compliance.

In Table 2 we reported the numerical results of the optimization of the cantilever using the method of polyhedral approximation with three increasing degrees of precision, as well as the results of the subdifferential technique. The graph showing the progressive decrease of the volume of the structure is presented in Figure 10a, while Figure 10b follows the evolution of the constraint in each numerical example.

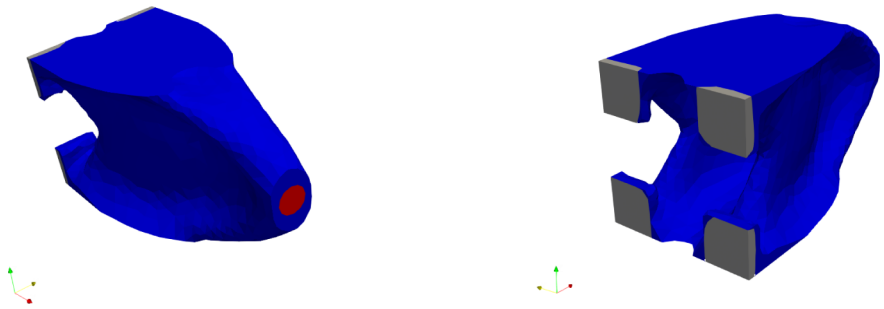

FIG. 8. *Optimal shape Ω_S resulting from the subdifferential approach.*

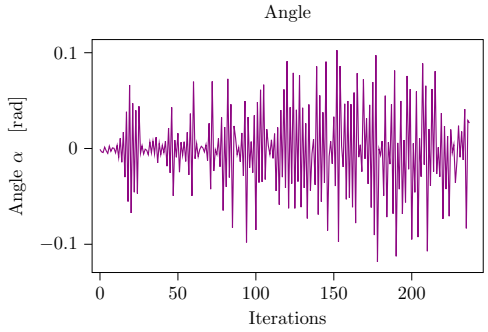

FIG. 9. *Evolution of the direction of the maximal constraint (in terms of the angle α) during the optimization process.*

A first remark concerns the slow rate of convergence of the four examples, as shown in Figure 10a. This issue seems to be proper to the 3D cantilever structure, as pointed out also in [33, section 6.2.1]. It seems that, nearing the end of the optimization, the directions of the shape derivatives of the objective and of the constraint are almost opposite one another. This issue slows down the convergence of the *nullspace optimization* algorithm by reducing the length of the optimization step to pass from one iteration to the next. Moreover, a small reduction in the volume of the structure entails a corresponding rise in the value of the compliance, leading to the violation of the inequality constraint.

For the simulations considered in this section we introduced a stopping criterion based on the merit function proper to the *nullspace optimization* algorithm introduced in [34]: the optimization algorithm terminates when the merit function passing from one iteration to the next increases for an increment equal to 2^{-6} times the original increment `dt`. Next, we can observe in Figure 10b that in all four cases the constraint on the maximum of the compliance is satisfied. By comparing the duration of the four simulations we can state that the method based on the subdifferential is efficient and reliable to solve problem (4.3) since it yields a result similar to the three other simulations while requiring fewer computations of the shape derivative.

Finally, we can see that the four simulations yield similar results, as a consequence of the preeminence of the vertical load to the optimization of the structure. The fact that the Hausdorff distances between Ω_N and Ω_S is of the order of the mesh size for each $N \in \{4, 8, 16\}$ supports the conclusion that all four simulations have reached a result close to the exact solution of problem (4.3).

TABLE 2

Numerical results for the optimization of the volume of the cantilever under constraints on the mechanical compliance, obtained using the polyhedron method (with an increasing number of vertices) and the subdifferential method.

		Polyhedron			
		$N=4$	$N=8$	$N=16$	**Subdifferential**
Optimization					
Duration	[min]	48	51	67	57
Number of iterations		239	239	291	237
Results					
Final volume Vol(Ω)	[cm^3]	0.5377	0.5377	0.4880	0.5503
Maximal compliance	[kPa cm^3]	0.0249	0.0249	0.0252	0.025 03
$\mathrm{d_H}(\Omega_S, \Omega_N)$	[cm]	0.1391	0.1391	0.1380	–

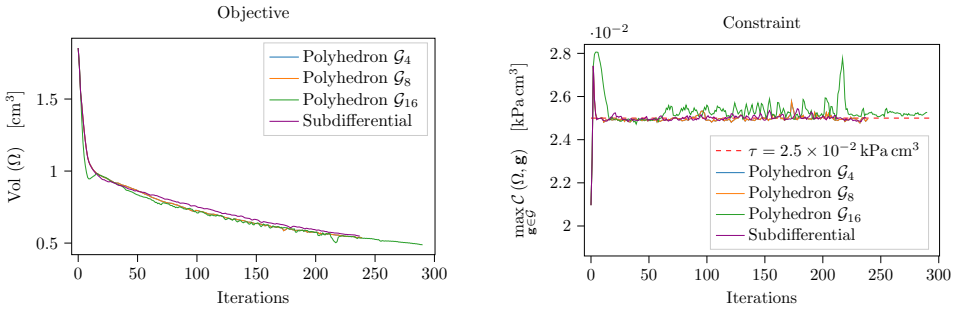

(a) Evolution of the objective function.

(b) Evolution of the constraint for three instances of the polyhedron method, and the method of the subdifferential.

FIG. 10. *Convergence of the objective (volume) and the constraint (compliance) for the cantilever.*

4.4. Bracket. As a final test, we applied the polyhedron method and the method of the subdifferential to a more realistic mechanical structure. We selected the bracket shown in Figure 11, inspired by the challenge proposed by General Electric in 2013 [1]. We suppose the bracket to be fixed on the four corners (marked in gray in Figure 11) by screws. A uniform mechanical load $\mathbf{g}$ is applied on the surface Γ_{N} on the upper grips. The intensity and direction of the applied load are unknown. However, we suppose that the vector $\mathbf{g}$ belongs to an ellipsoid $\mathcal{G}$ whose semiaxes correspond to the maximal admissible loads in the directions x, y, and z:

$$\frac{X^2}{\overline{g}_x^2} + \frac{Y^2}{\overline{g}_y^2} + \frac{Z^2}{\overline{g}_z^2} \leq 1, \tag{4.9}$$

where $\mathbf{g} = X\mathbf{e}_x + Y\mathbf{e}_y + Z\mathbf{e}_z$.

As for the cantilever studied in subsection 4.3, we aim to minimize the volume of the structure under a constraint on the maximum possible value of the mechanical compliance. The material properties of the structure, its dimensions, and the threshold on the compliance in the optimization problem are reported in Table 6 in the appendix.

In the three instances of the polyhedron method presented for this case, we approximated the ellipsoid $\mathcal{G}$ by the polyhedra $\mathcal{G}_8$, $\mathcal{G}_{12}$, and $\mathcal{G}_{20}$. These polyhedra have

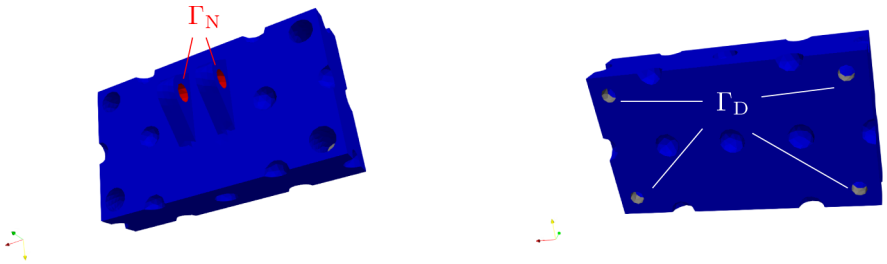

FIG. 11. *Structure of the bracket. The structure is clamped on the four corners Γ_D marked in gray. A uniform load of uncertain intensity and direction is applied on the red region Γ_N. (Color available online.)*

TABLE 3

Numerical results for the optimization of the volume of the jet bracket under constraints on the mechanical compliance, obtained using the polyhedron method and the subdifferential method.

		Polyhedron			
		$N=6$	$N=12$	$N=20$	**Subdifferential**
Optimization					
Duration	[min]	78	88	94	62
Number of iterations		100	100	100	100
Results					
Final volume Vol(Ω)	[cm^3]	249 627	247 369	259 371	262 900
Maximal compliance	[MPa cm^3]	0.030 044	0.030 212	0.030 018	0.030 694
$d_H(\Omega_S,\Omega_N)$	[cm]	12.32	12.56	8.650	–

been obtained by applying to a regular octahedron, a cube, and a regular dodecahedron the same linear transformation mapping the circumscribed sphere to the ellipsoid $\mathcal{G}$. The computation of the admissible load $\overline{\mathbf{g}}$ maximizing the constraint functional is necessary for the execution of the method of the subdifferential. Thanks to the quadratic nature of the compliance functional, $\overline{\mathbf{g}}$ can be found by computing the eigenvector $\mathbf{v}$ associated to the maximal eigenvalue of the symmetric matrix $\mathbf{M}_\Omega \in \mathbb{R}^{3\times 3}$ such that

$$[\mathbf{M}_\Omega]_{i,j} = \int_\Omega \boldsymbol{\sigma}(\mathbf{u}_i) : \boldsymbol{\varepsilon}(\mathbf{u}_j)\, \mathrm{d}\mathbf{x},$$

where $\mathbf{u}_1$, $\mathbf{u}_2$, and $\mathbf{u}_3$ are the displacements induced by $\overline{g}_x\mathbf{e}_x$, $\overline{g}_y\mathbf{e}_y$, and $\overline{g}_z\mathbf{e}_z$, respectively. Indeed, we have that

$$\overline{\mathbf{g}} = \arg\max_{\mathbf{g}\in\mathcal{G}} \mathcal{C}(\mathbf{u}_{\Omega,\mathbf{g}}, \Omega) = \mathbf{v}_1\overline{g}_x\mathbf{e}_x + \mathbf{v}_2\overline{g}_y\mathbf{e}_y + \mathbf{v}_3\overline{g}_z\mathbf{e}_z.$$

We present the trends of the objective and the maximal constraint for the four numerical examples in Figures 12a and 12b, respectively. The numerical results are compiled in Table 3, and the resulting optimal structures are shown in Figure 13. The graphs of Figure 12 show that all four examples converge to an optimal solution around the sixtieth iteration. We denote by Ω_6, Ω_{12}, and Ω_{20} the optimal structures obtained by the three instances of the polyhedron method, and by Ω_S the optimal shape obtained by the method of the subdifferential. The faster convergence of the

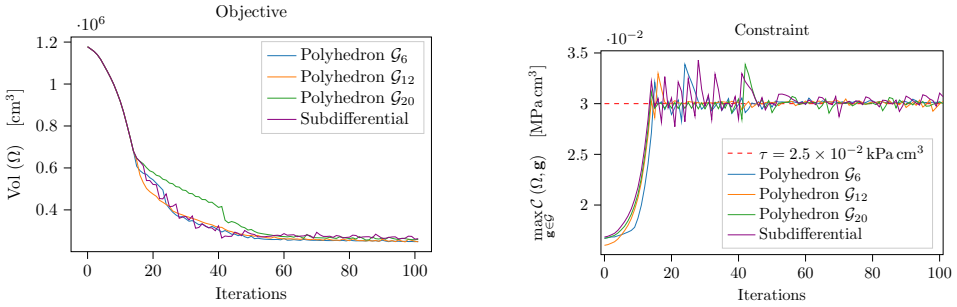

(a) Evolution of the objective (volume).

(b) Evolution of the constraint (mechanical compliance).

FIG. 12. *Convergence of the objective (volume) and the constraint for the jet bracket.*

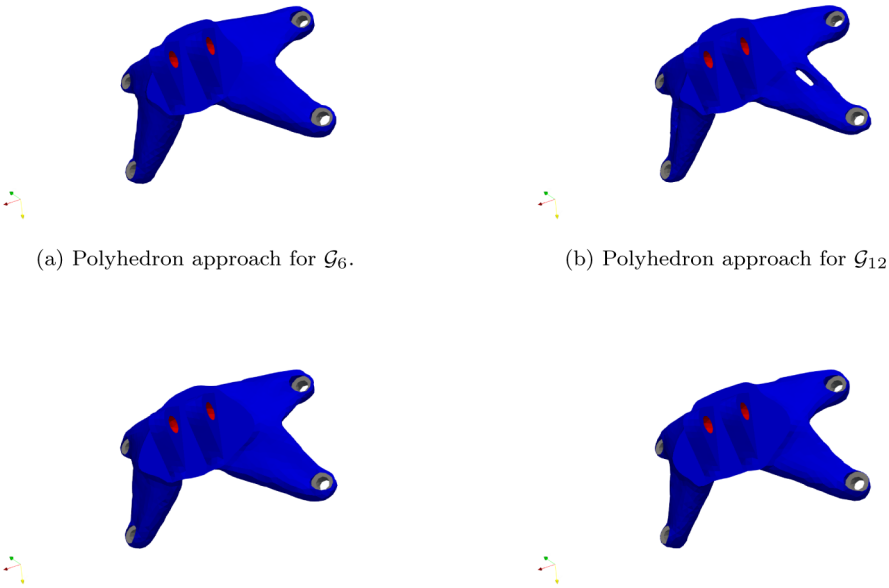

(a) Polyhedron approach for $\mathcal{G}_6$.

(b) Polyhedron approach for $\mathcal{G}_{12}$.

(c) Polyhedron approach for $\mathcal{G}_{20}$.

(d) Subdifferential approach.

FIG. 13. *Optimal shape of the jet bracket for the polyhedron and subdifferential approaches.*

algorithm for the bracket with respect to the disc considered in subsection 4.2 can be explained by the fact that the bracket is characterized only by a planar symmetry, and the direction of the larger constraint is consistent throughout the optimization. In all four cases we obtain an optimal structure with four branches connecting the clamped supports to the grips where the load is applied. As shown in Table 3, the four optimal structures respect the constraint on the maximal value of the mechanical compliance. The values of the objective function and the decrease of the Hausdorff distance between Ω_S and the structures Ω_6, Ω_{12}, and Ω_{20} confirm the theoretical results of Theorem 2.7.

5. Conclusions and perspectives. In this paper we have compared two different methods for solving shape optimization problems under worst-case constraints on a given function. The first method can only be applied to convex functions of the displacement, and is based on the approximation of the set $\mathcal{G}$ of admissible loads by polyhedra. This method is effectively the design of a structure that satisfies the constraint in a finite number of representative load cases. The second method is based on the calculation of an element of the subdifferential of the constraint by identifying the critical element of the $\mathcal{G}$ that maximizes the constraint and differentiating in the relative direction.

The numerical simulations of section 4 support the effectiveness of both methods in the case of an admissible set of loads parameterized by an ellipse in $\mathbb{R}^2$. We observed that in both cases the subdifferential method is faster than the polyhedral approximation, since it requires fewer evaluations of the constraint function. However, we note that when the allowable load maximizing the constraint is not unique, the convergence of the subdifferential method is degraded and smaller, and more numerous optimization steps are required to converge.

One way to improve the subdifferential method is to consider multiple elements of the subdifferential of the constraint function. Such a variant of the algorithm would require identifying whether multiple mechanical loads maximize the constraint for a given shape. A possible direction of development could be the adaptation of the proximal algorithm to shape optimization, since it already relies on the subdifferential in the sense of Clarke. See [8, 44, 40] and references therein for further information on the proximal algorithm in nonsmooth optimization.

Appendix A. Parameters for the numerical experiments.

TABLE 4
Numerical data concerning the geometry and the mechanics of the disc structure of Figure 2.

Geometry of the structure		
height of the domain		12.0 cm
maximal radius of the domain		12.0 cm
Region Γ_N		
inner radius of Γ_N		4.0 cm
outer radius of Γ_N		6.0 cm
Region Γ_D		
thickness of Γ_D		2.0 cm
Mesh size parameters		
minimal mesh size	`hmin`	0.75 cm
maximal mesh size	`hmax`	1.25 cm
Elastic coefficients		
Young's modulus	E	200 MPa
Poisson's ratio	ν	0.3
Mechanical loads		
maximal load in any direction	$\overline{g}$	10 kPa
threshold on $\|s_D\|_6$	τ	5.0 kPa

TABLE 5
Numerical data concerning the geometry and the mechanics of the cantilever of Figure 6.

Geometry of the structure		
cross section length	ℓ_s	1.0 cm
longitudinal length	ℓ_x	2.0 cm
sidelength of Γ_{D}		0.3 cm
radius of Γ_{N}		0.1 cm
Elastic coefficients		
Young's modulus	E	200 MPa
Poisson's ratio	ν	0.3
Mechanical loads		
compression load	$\overline{g}_x$	25 kPa
vertical load	$\overline{g}_z$	10 kPa
Mesh size parameters		
minimal mesh size	`hmin`	0.025 cm
maximal mesh size	`hmax`	0.10 cm
Thresholds for the inequality constraints		
threshold on the compliance	τ	2.5×10^{-2} kPa cm^3
bound on the probability of failure	$\bar{p}$	1.0%

TABLE 6
Numerical data concerning the geometry and the mechanics of the bracket of Figure 11.

Geometry of the structure		
Length	ℓ_x	210 cm
Depth	ℓ_y	120 cm
Height	ℓ_z	50 cm
Side length of Γ_{D}		0.2 cm
Side length of each Γ_{N}^i		1.0 cm
Mesh size parameters		
Minimal mesh size	`hmin`	4 cm
Maximal mesh size	`hmax`	6 cm
Elastic coefficients		
Young's modulus	E	200 MPa
Poisson's ratio	ν	0.3
Mechanical loads		
Intensity of the maximal mechanical load	$\overline{g}_x = \overline{g}_y = \overline{g}_z$	1 MPa
Thresholds for the inequality constraints		
Threshold on the compliance	τ_C	3.0×10^{-2} MPa cm^3

REFERENCES

[1] *GE Jet Engine Bracket Challenge | Engineering & Design Challenges | GrabCAD*, https://grabcad.com/challenges/ge-jet-engine-bracket-challenge.

[2] S. ADLY, L. BOURDIN, F. CAUBET, AND A. J. DE CORDEMOY, *Shape optimization for variational inequalities: The scalar Tresca friction problem*, SIAM J. Optim., 33 (2023), pp. 2512–2541, https://doi.org/10.1137/22M1497560.

[3] G. ALLAIRE AND C. DAPOGNY, *A linearized approach to worst-case design in parametric and geometric shape optimization*, Math. Models Methods Appl. Sci., 24 (2014), pp. 2199–2257, https://doi.org/10.1142/S0218202514500195.

[4] G. ALLAIRE AND C. DAPOGNY, *A deterministic approximation method in shape optimization under random uncertainties*, SMAI J. Comput. Math., 1 (2015), pp. 83–143, https://doi.org/10.5802/smai-jcm.5.

[5] G. Allaire and F. Jouve, *A level-set method for vibration and multiple loads structural optimization*, Comput. Methods Appl. Mech. Engrg., 194 (2005), pp. 3269–3290, https://doi.org/10.1016/j.cma.2004.12.018.

[6] G. Allaire, F. Jouve, and G. Michailidis, *Thickness control in structural optimization via a level set method*, Struct. Multidiscip. Optim., 53 (2016), pp. 1349–1382, https://doi.org/10.1007/s00158-016-1453-y.

[7] S. Amstutz and M. Ciligot-Travain, *A notion of compliance robustness in topology optimization*, ESAIM Control Optim. Calc. Var., 22 (2016), pp. 64–87, https://doi.org/10.1051/cocv/2014066.

[8] H. Attouch and J. Bolte, *On the convergence of the proximal algorithm for nonsmooth functions involving analytic features*, Math. Program., 116 (2009), pp. 5–16, https://doi.org/10.1007/s10107-007-0133-5.

[9] H. Attouch and R. J.-B. Wets, *Quantitative stability of variational systems:* I. *The epigraphical distance*, Trans. Amer. Math. Soc., 328 (1991), pp. 695–729, https://doi.org/10.2307/2001800, 1991.

[10] G. Augusti, J. B. Martin, and W. Prager, *On the decomposition of stress and strain tensors into spherical and deviatoric parts*, Proc. Natl. Acad. Sci. USA, 63 (1969), pp. 239–241.

[11] G. Balarac, F. Basile, P. Bénard, F. Bordeu, J.-B. Chapelier, L. Cirrottola, G. Caumon, C. Dapogny, P. Frey, A. Froehly, G. Ghigliotti, R. Laraufie, G. Lartigue, C. Legentil, R. Mercier, V. Moureau, C. Nardoni, S. Pertant, and M. Zakari, *Tetrahedral remeshing in the context of large-scale numerical simulation and high performance computing*, MathS in Action, 11 (2022), pp. 129–164, https://doi.org/10.5802/msia.22.

[12] I. Bárány and Z. Füredi, *Approximation of the sphere by polytopes having few vertices*, Proc. Amer. Math. Soc., 102 (1988), pp. 651–659, https://doi.org/10.2307/2047241.

[13] A. Ben-Tal, L. E. Ghaoui, and A. Nemirovski, *Robust optimization*, in Robust Optimization, Princeton University Press, 2009, https://doi.org/10.1515/9781400831050.

[14] A. Ben-Tal and A. Nemirovski, *Robust optimization: Methodology and applications*, Math. Program., 92 (2002), pp. 453–480, https://doi.org/10.1007/s101070100286.

[15] C. T. T. Bui, C. Dapogny, and P. Frey, *An accurate anisotropic adaptation method for solving the level set advection equation*, Internat. J. Numer. Methods Fluids, 70 (2012), pp. 899–922, https://doi.org/10.1002/fld.2730.

[16] F. Caubet, M. Dambrine, and R. Mahadevan, *Shape derivative for some eigenvalue functionals in elasticity theory*, SIAM J. Control Optim., 59 (2021), pp. 1218–1245, https://doi.org/10.1137/20M1343105.

[17] F. Caubet, M. Dambrine, and R. Mahadevan, *Shape sensitivity of eigenvalue functionals for scalar problems: Computing the semi-derivative of a minimum*, Appl. Math. Optim., 86 (2022), 10, https://doi.org/10.1007/s00245-022-09827-6.

[18] S. Chen, W. Chen, and S. Lee, *Level set based robust shape and topology optimization under random field uncertainties*, Struct. Multidiscip. Optim., 41 (2010), pp. 507–524, https://doi.org/10.1007/s00158-009-0449-2.

[19] D. Chenais, *On the existence of a solution in a domain identification problem*, J. Math. Anal. Appl., 52 (1975), pp. 189–219, https://doi.org/10.1016/0022-247X(75)90091-8.

[20] E. Cherkaev and A. Cherkaev, *Principal compliance and robust optimal design*, J. Elasticity, 72 (2003), pp. 71–98, https://doi.org/10.1023/B:ELAS.0000018772.09023.6c.

[21] F. H. Clarke, *Optimization and Nonsmooth Analysis*, Classics Appl. Math. 5, SIAM, Philadelphia, 1990, https://doi.org/10.1137/1.9781611971309.

[22] M. Dambrine, C. Dapogny, and H. Harbrecht, *Shape optimization for quadratic functionals and states with random right-hand sides*, SIAM J. Control Optim., 53 (2015), pp. 3081–3103, https://doi.org/10.1137/15M1017041.

[23] M. Dambrine, H. Harbrecht, and B. Puig, *Incorporating knowledge on the measurement noise in electrical impedance tomography*, ESAIM Control Optim. Calc. Var., 25 (2019), 84, https://doi.org/10.1051/cocv/2018010.

[24] M. Dambrine, D. Kateb, and J. Lamboley, *An extremal eigenvalue problem for the Wentzell–Laplace operator*, Ann. Inst. H. Poincaré C Anal. Non Linéaire, 33 (2016), pp. 409–450, https://doi.org/10.1016/j.anihpc.2014.11.002.

[25] M. Dambrine and A. Laurain, *A first order approach for worst-case shape optimization of the compliance for a mixture in the low contrast regime*, Struct. Multidiscip. Optim., 54 (2016), pp. 215–231, https://doi.org/10.1007/s00158-015-1384-z.

[26] M. Dambrine and S. Zerrouq, *Robust inverse homogenization of elastic microstructures*, J. Optim. Theory Appl., 199 (2023), pp. 209–232, https://doi.org/10.1007/s10957-023-02266-5.

[27] J. M. Danskin, *The theory of Max-Min, with applications*, SIAM J. Appl. Math., 14 (1966), pp. 641–664, https://doi.org/10.1137/0114053.
[28] C. Dapogny, C. Dobrzynski, and P. Frey, *Three-dimensional adaptive domain remeshing, implicit domain meshing, and applications to free and moving boundary problems*, J. Comput. Phys., 262 (2014), pp. 358–378, https://doi.org/10.1016/j.jcp.2014.01.005.
[29] C. Dapogny and F. Feppon, *Shape optimization using a level set based mesh evolution method: An overview and tutorial*, C. R. Math., 361 (2023), pp. 1267–1332, https://doi.org/10.5802/crmath.498.
[30] C. Dapogny and P. Frey, *Computation of the signed distance function to a discrete contour on adapted triangulation*, Calcolo, 49 (2012), pp. 193–219, https://doi.org/10.1007/s10092-011-0051-z.
[31] F. de Gournay, G. Allaire, and F. Jouve, *Shape and topology optimization of the robust compliance via the level set method*, ESAIM Control Optim. Calc. Var., 14 (2008), pp. 43–70, https://doi.org/10.1051/cocv:2007048.
[32] M. C. Delfour and J.-P. Zolésio, *Shapes and Geometries: Metrics, Analysis, Differential Calculus, and Optimization*, 2nd ed., Adv. Design Control 22, SIAM, Philadelphia, 2011, https://doi.org/10.1137/1.9780898719826.
[33] F. Feppon, *Optimisation Topologique de Systèmes Multiphysiques*, Ph.D. thesis, Université Paris Saclay (COmUE), 2019.
[34] F. Feppon, G. Allaire, and C. Dapogny, *Null space gradient flows for constrained optimization with applications to shape optimization*, ESAIM Control Optim. Calc. Var., 26 (2020), 90, https://doi.org/10.1051/cocv/2020015.
[35] K. Gao, D. M. Do, S. Chu, G. Wu, H. A. Kim, and C. A. Featherston, *Robust topology optimization of structures under uncertain propagation of imprecise stochastic-based uncertain field*, Thin-Walled Structures, 175 (2022), 109238, https://doi.org/10.1016/j.tws.2022.109238.
[36] X. Guo, W. Zhang, and L. Zhang, *Robust structural topology optimization considering boundary uncertainties*, Comput. Methods Appl. Mech. Engrg., 253 (2013), pp. 356–368, https://doi.org/10.1016/j.cma.2012.09.005.
[37] A. Habbal, *Nonsmooth shape optimization applied to linear acoustics*, SIAM J. Optim., 8 (1998), pp. 989–1006, https://doi.org/10.1137/S105262349529581X.
[38] F. Hecht, *New development in FreeFEM++*, J. Numer. Math., 20 (2012), pp. 1–14, https://doi.org/10.1515/jnum-2012-0013.
[39] A. Henrot and M. Pierre, *Shape Variation and Optimization: A Geometrical Analysis*, Tracts Math. 28, European Mathematical Society, Zurich, 2018.
[40] L. Hertlein and M. Ulbrich, *An inexact bundle algorithm for nonconvex nonsmooth minimization in Hilbert space*, SIAM J. Control Optim., 57 (2019), pp. 3137–3165, https://doi.org/10.1137/18M1221849.
[41] R. M. Jones, *Deformation Theory of Plasticity*, Bull Ridge Corporation, Blacksburg, VA, 2008.
[42] T. Lassila, A. Manzoni, A. Quarteroni, and G. Rozza, *Boundary control and shape optimization for the robust design of bypass anastomoses under uncertainty*, ESAIM Math. Model. Numer. Anal., 47 (2013), pp. 1107–1131, https://doi.org/10.1051/m2an/2012059.
[43] D. Luft, V. H. Schulz, and K. Welker, *Efficient techniques for shape optimization with variational inequalities using adjoints*, SIAM J. Optim., 30 (2020), pp. 1922–1953, https://doi.org/10.1137/19M1257226.
[44] D. Noll, *Convergence of non-smooth descent methods using the Kurdyka–Łojasiewicz inequality*, J. Optim. Theory Appl., 160 (2014), pp. 553–572, https://doi.org/10.1007/s10957-013-0391-8.
[45] R. T. Rockafellar, *Convex Analysis*, Princeton Math. Ser., Princeton University Press, 1970, https://doi.org/10.1515/9781400873173.